Geophysical Research Letters

RESEARCH LETTER
10.1029/2021GL092939

Statistical Modeling of the Bering Strait Throughflow for Operational Sea Ice Forecasting in the Chukchi Sea

Jed E. Lenetsky[1,2] **and Mark C. Serreze**[1,2]

[1]National Snow and Ice Data Center, Cooperative Institute for Research in Environmental Sciences, University of Colorado, Boulder, CO, USA, [2]Department of Geography, University of Colorado, Boulder, Boulder, CO, USA

Key Points:

- Variability in Bering Strait volume transports can be captured using surface winds and Ekman transports in the East Siberian and Bering Seas
- Bering Sea sea surface temperatures, along with modeled volume transports, can capture Bering Strait ocean heat transport variability
- Modeled ocean heat transports can be used to skillfully forecast sea ice retreat and advance dates with 1 and 4-month lead times

Correspondence to:
J. E. Lenetsky,
jed.lenetsky@colorado.edu

Citation:
Lenetsky, J. E., & Serreze, M. C. (2021). Statistical modeling of the Bering Strait throughflow for operational sea ice forecasting in the Chukchi Sea. *Geophysical Research Letters*, *48*, e2021GL092939. https://doi.org/10.1029/2021GL092939

Received 10 FEB 2021
Accepted 27 APR 2021
Corrected 28 MAY 2021

This article was corrected on 28 MAY 2021. See the end of the full text for details.

© 2021. American Geophysical Union. All Rights Reserved.

Abstract We utilize statistically modeled ocean heat transports through the Bering Strait along with additional predictors to create skillful predictions of sea ice retreat and advance dates in the Chukchi Sea. Interannual variability of June and September oceanic heat transports through the strait can be captured using modeled Ekman transports, surface winds, and sea surface temperatures. At one-month leads, our models can explain 41% and 79% of sea ice retreat and advance date variance with root mean squared errors (RMSEs) of 10.2 and 12.8 days respectively. At 4-month leads, our models can respectively capture 37% and 73% of sea ice retreat and advance date variance with RMSEs of 8.5 and 14.6 days. These findings offer a path toward operational forecasts of sea ice retreat and advance dates in the Chukchi Sea in the absence of direct, readily available observations of heat transports in the strait.

Plain Language Summary The Chukchi Sea is a key region for shipping and other growing economic activities in the Arctic. Seasonal sea ice conditions in the region are strongly determined by the oceanic heat transport into the Chukchi Sea from the north Pacific Ocean via the Bering Strait. However, seasonal predictions of sea ice are hampered by the lack of high quality, real-time, observations of Bering Strait water properties. We address this limitation by statistically modeling Bering Strait volume and heat transports and then using these models to forecast sea ice retreat and advance dates in the Chukchi Sea. Skillful sea ice forecasts in this critical region have the potential to increase the navigability of Arctic waters.

1. Introduction

The Arctic Ocean is becoming increasingly accessible to oil and natural gas exploration, marine shipping, tourism, and commercial fishing (United States Navy, 2014). The Chukchi Sea is especially important in this regard; it is resource rich and vessels transiting the Arctic Ocean must pass through it. Consequently, there has been increasing interest in the seasonal forecasting of sea ice conditions in the Chukchi Sea at lead times relevant to stakeholders (Serreze & Meier, 2019).

The Chukchi Sea connects to the North Pacific Ocean via the narrow Bering Strait, through which there is a northward transport of comparatively fresh (~32 psu), warm (in spring, summer, and fall) Pacific Waters (Woodgate, 2018). Bering Strait water temperature, volume transport, and salinity has been continuously monitored via mooring arrays since 1998 (Woodgate, 2018). Past studies have linked the Bering Strait inflow to sea ice conditions in the Chukchi Sea (Ahlnas & Garrison, 1984; Lenetsky et al., 2021; Paquette & Bourke, 1974; Serreze et al., 2016; Spall, 2007; Woodgate et al., 2010, 2015). Large ocean heat transports (OHT) in the spring provide an early source of bottom melt across the Chukchi Sea, providing a trigger for the ice-albedo feedback and extensive summer ice melt (Lenetsky et al., 2021; Woodgate et al., 2010). The spring Bering Strait OHT based on mooring data can explain 2/3 of the variance in the timing of the seasonal ice retreat in the Chukchi Sea (Serreze et al., 2016). The July through September mean OHT, along with the date of ice retreat, explains 2/3 of the of freeze onset variability (Serreze et al., 2016).

Variability in the Bering Strait OHT is determined by both water temperature and volume transport (T_{vol}). Recent increases in Bering Strait near-bottom water temperatures broadly parallel global increases in ocean heat content (Woodgate, 2018), but interannual variability is less understood. There are links between the strength of the wintertime atmospheric polar vortex over the North Pacific Ocean and sea surface temperature (SST) anomalies in the Bering Sea (Zhang et al., 2019), as well as the phase of the Pacific Decadal Oscillation (Clement et al., 2005; Serreze et al., 2019), but physical connections remain unclear.

Mechanisms driving variability in the Bering Strait T_{vol} are more straightforward. On average, mean southward, along strait winds partly counter a northward, pressure-head driven flow formed by sea surface height differences between the Pacific and Arctic Oceans. The pressure-head flow is a significant source of Bering Strait T_{vol} variability (Woodgate, 2018). Variable sea surface height gradients between the Bering Sea and Arctic Ocean are set by sea level pressure patterns in both the Bering Sea and central Arctic Ocean. Positive sea surface height anomalies in the Bering Sea are associated with a westward displaced Aleutian Low driving northeast Ekman transports and a convergence of water along the Alaskan-Bering Sea coastline, whereas low sea surface height anomalies are associated with an eastward displaced Aleutian Low (Danielson et al., 2014; Zhang et al., 2020). In the Arctic, sea surface heights in the East Siberian Sea (ESS), controlled by zonal winds along the Siberian coastline forcing off-shore or on-shore Ekman transport, are also critically important in driving variability in the pressure-head flow (Danielson et al., 2014; Peralta-Ferriz & Woodgate, 2017). Winds in the ESS and the T_{vol} through the Bering Strait are both linked to larger scale atmospheric circulation patterns broadly associated with the summer Arctic Oscillation (AO) pattern (Serreze et al., 2019). The relative strength of the atmospheric forcing between the Bering and ESSs exhibits decadal variability: in some decades (2000s and 2010s), the Arctic atmospheric circulation played a dominant role (Peralta-Ferriz & Woodgate, 2017), whereas in others (1980s and 1990s), winds in the Bering and ESSs were roughly equal in importance (Zhang et al., 2020).

Despite growing process understanding, operational forecasting of ice conditions in the Chukchi Sea is hampered by long latency in data retrieval from moorings; retrieval requires a site visit. We address this challenge by developing statistical models that capture the spring and summer interannual variability in Bering Strait T_{vol} using along-strait winds and regionally averaged Ekman transports over the East Siberian and Bering Seas. We investigate the ability of SSTs to capture variability in observed water temperatures and total OHT. Variables from these OHT parameterizations ($\widehat{\mathrm{OHT}}$) are then used to produce models of Chukchi Sea ice retreat and advance dates with lead times of 1 and 4 months.

2. Data and Methods

2.1. Bering Strait OHT

The observed monthly mean Bering Strait OHT is derived from hourly, corrected, near-bottom temperature and transport observations from 1998 to 2018 from the A3 mooring, deployed 35 km north of the Bering Strait at a depth of 57 m (Woodgate, 2018; Woodgate et al., 2015, Woodgate & Peralta-Ferriz, 2021). The monthly mean Bering Strait OHT is:

$$OHT = \rho_w T_{vol} C_w \left(\theta - \theta_{ref}\right) \quad (1)$$

where, ρ_w is the seawater density (1,023 kg m^{-3}), T_{vol} is the volume transport through the strait, C_w is the specific heat capacity of water (3900 J $kg^{-1}K^{-1}$), Θ is the water temperature, and Θ_{ref} is the reference freezing point temperature (−1.9°C; Woodgate, 2018). The pressure-head component of T_{vol} (no local winds) is approximated from the residual of correlations between 6-hour water velocities in the strait and along-strait winds at one year windows (see Woodgate, 2018 for details).

2.2. Ekman Transports

Past calculations of Ekman transport and pumping in the Arctic have involved explicitly differentiating between the stresses applied to the surface by winds and a moving ice cover (Meneghello et al., 2018; Timmermans et al., 2014; Yang, 2006). These studies utilized NSIDC Polar Pathfinder sea ice motion vectors, but this data set is not regularly updated. We hence use a parameterization from Lüpkes and Birnbaum (2005), in which the total stress on the surface over a given area is a function of winds and sea ice concentration (SIC) alone. The stress from weighting the surface stress coefficient C_{Dt} by SIC is:

$$C_{Dt} = \left(0.34A^2\right)\frac{\left(1-A\right)^{0.8} + 0.5\left(1-0.5A\right)^2}{a_r + 90} + \mathrm{A}^{*} C_{Di} + \left(1-A\right) * C_{Da} \quad (2)$$

where A is equal to the SIC, C_{Di} and C_{Da} are the fixed drag coefficients of ice (1.89×10^{-3}) and air (1.25×10^{-3}) on ocean water. a_r is the aspect ratio, relating the length of a sea ice floe to its thickness. a_r is calculated using:

$$a_r = \mathrm{D}_i \,/\, h_f \tag{3}$$

where and D_i is the flow length and h_f is the sea ice freeboard. D_i and h_f are each estimated by:

$$D_i = 31 * \frac{h_f}{1 - A} \tag{4}$$

$$h_f = 0.49 * \left(1 - e^{-5.9A}\right) \tag{5}$$

In these estimates, floe lengths vary from 4 to 300 m, for $A = 0.05$ and $A = 0.95$ respectively, while freeboard heights vary from 0.13 m for $A = 0.05$ to 0.49 m when $A = 0.95$ (Lüpkes & Birnbaum, 2005). Equation 2 is derived using previous approximations of sea ice form drag over the ocean surface (Birnbaum & Lüpkes, 2002), and fitting the approximations to observational measurements of form drag during the REFLEX air campaign in the Fram Strait (Lüpkes & Birnbaum, 2005).

After determining the drag coefficient based on SIC, a quadratic drag law is used to calculate the surface stress on the ocean surface:

$$\tau_x = \rho C_{Dt} \left|U_{10m}\right| \left(U_{10m}\right) \tag{6}$$

$$\tau_y = \rho C_{Dt} \left|V_{10m}\right| \left(V_{10m}\right) \tag{7}$$

where ρ is the average density of ocean water at 1,023 kg m^{-3}; U_{10m} and V_{10m} are the ERA5 10-meter wind components (Hersbach et al., 2020). Wanting to use continuously and regularly updated data sources, we neglect upper ocean currents in our surface stress calculations, which may introduce additional errors in modeled Ekman transports. From there, Ekman transport vectors ($m^2 s^{-1}$) are computed following Pond and Pickard (1978):

$$V_{Ek} = -\frac{\tau_x}{\rho f} \tag{8}$$

$$U_{Ek} = \frac{\tau_y}{\rho f} \tag{9}$$

where f is the Coriolis parameter.

Ekman transport vectors are calculated at each ERA5 grid cell, then averaged over the Bering Sea continental shelf (60°N–65°N, 165°W–180°W) and ESS (75°N–80°N, 140°E–180°W) regions (Figure 1). The ESS region corresponds to the area of maximum correlation between summer zonal wind anomalies and the principal component of the first EOF mode of GRACE ocean bottom pressure anomalies calculated in Peralta-Ferriz and Woodgate (2017). This region agrees with composite plots of Ekman transports for months with large and small pressure-head flows (Figure 1). For months with large pressure-head flows, Ekman transports are primarily northward and offshore in the ESS region, whereas for low pressure-head flow months, Ekman transports are southward and onshore (Figures 1b–1d). A similar pattern emerges within the Bering Sea region - high flow months are associated with northwestward Ekman transports, whereas lower flow months are associated with westward and weaker northward transports (Figures 1b–1d). The exact direction of composite mean Ekman transports in the Bering Sea differ from previous studies (Danielson et al., 2014; Zhang et al., 2020), in which larger pressure-head flows were associated with northeastward, not northwestward, Ekman transports toward the Alaskan coastline. We attribute this discrepency to the relatively weak Bering Sea wind forcing compared to the ESS region throughout the mooring record, reducing the influence and importance of the exact direction of Ekman transports in the Bering Sea (Peralta-Ferriz & Woodgate, 2017). There is also considerable monthly variability in the direction of the transports in the

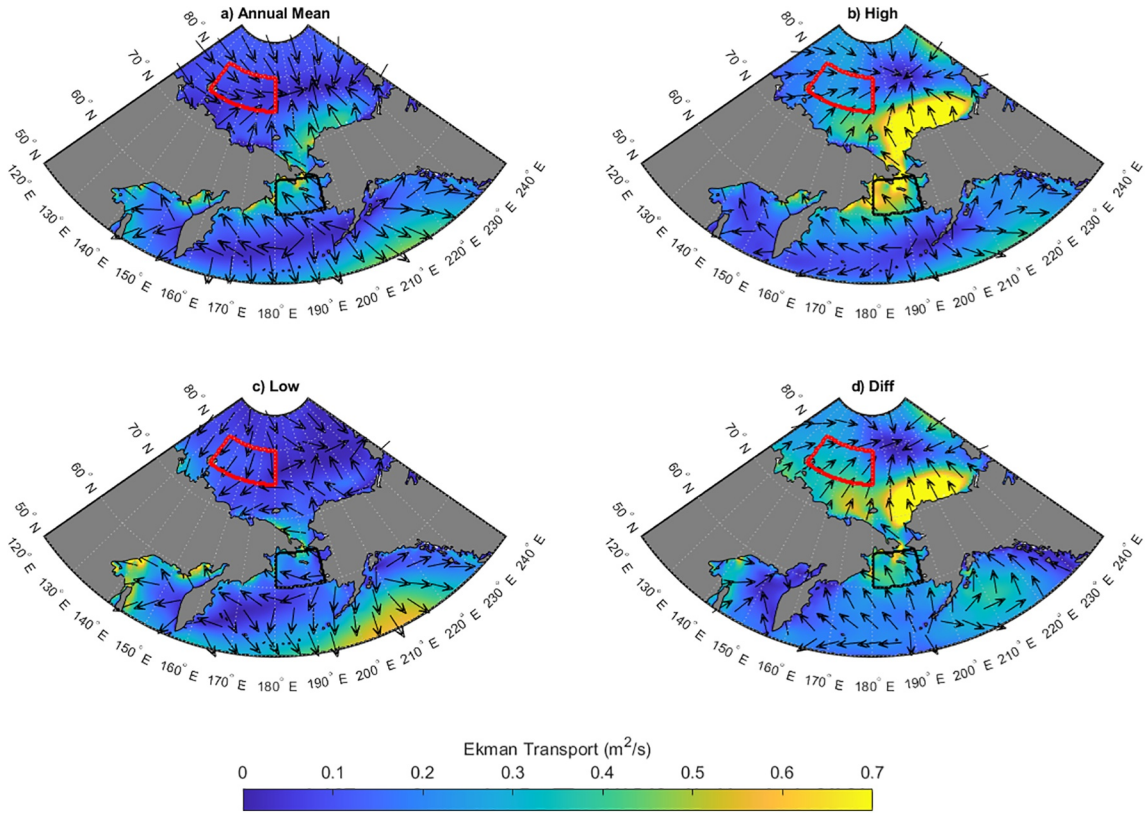

Figure 1. The 1998 through 2018 mean Ekman transport field for all (a) available months, (b) months with the 15 highest pressure-head flows, (c) the 15 lowest pressure-head flows, and (d) the difference between high and low flow months. The East Siberian Sea (ESS) region (75°N–80°N, 140°E–180°W) is shown in red and the Bering Sea region (60°N–65°N, 165°W–180°W) is shown in black.

Bering sea for large pressure-head flows: northwest in June, west in September, and northeast in July. Thus, for simplicity, we reconstruct Bering Strait T_{vol} variability using the mean meridional component of Ekman transport velocity (V_{Ek}) in the Bering Sea and ESS (roughly corresponding to an on/offshore transport) together with along-strait surface winds.

2.3. Calculation of Ice Retreat and Advance Dates

Ice retreat and advance dates from 1979 to 2018 are assessed following Serreze et al. (2016). We calculated regional averages (weighted by grid cell area) of daily SIC fields (Cavalieri et al., 1996) for the Chukchi Sea continental shelf bounded by the 150 m isobath (see Figure 2). Sea ice retreat date (RD) is defined as the first day of year that the average SIC falls below 30% and the advance date (AD) is the first day after the regional sea ice minimum when regionally averaged SIC exceeds 30%. The mean RD is July 14th and the mean AD is October 29th.

2.4. Model Building

Statistical models were built using the iterative process of forward selection, adding potential predictor variables to a linear regression of the form $\hat{y} = \alpha + \beta_1 X_1 + \beta_2 X_2 + \ldots + \beta_n X_n$ for n predictors. Here α is the y-intercept and β is the regression coefficient for a predictor variable X. The T_{vol} and OHT models began as null models in which the only predictor is α, to which Ekman transports and NOAA SSTs (ERSST v3b from 1979 to 1981 and OISST v2 from 1982 to 2018; Banzon et al., 2016; Huang et al., 2017; Smith & Reynolds, 2003) are added. Following Serreze et al. (2016), both RD and AD models begin with variables from the OHT models as a parameterization for the Bering Strait OHT. This avoids the compounding errors associated with using nested linear models as predictors. Our OHT models demonstrate that AD and RD model skills

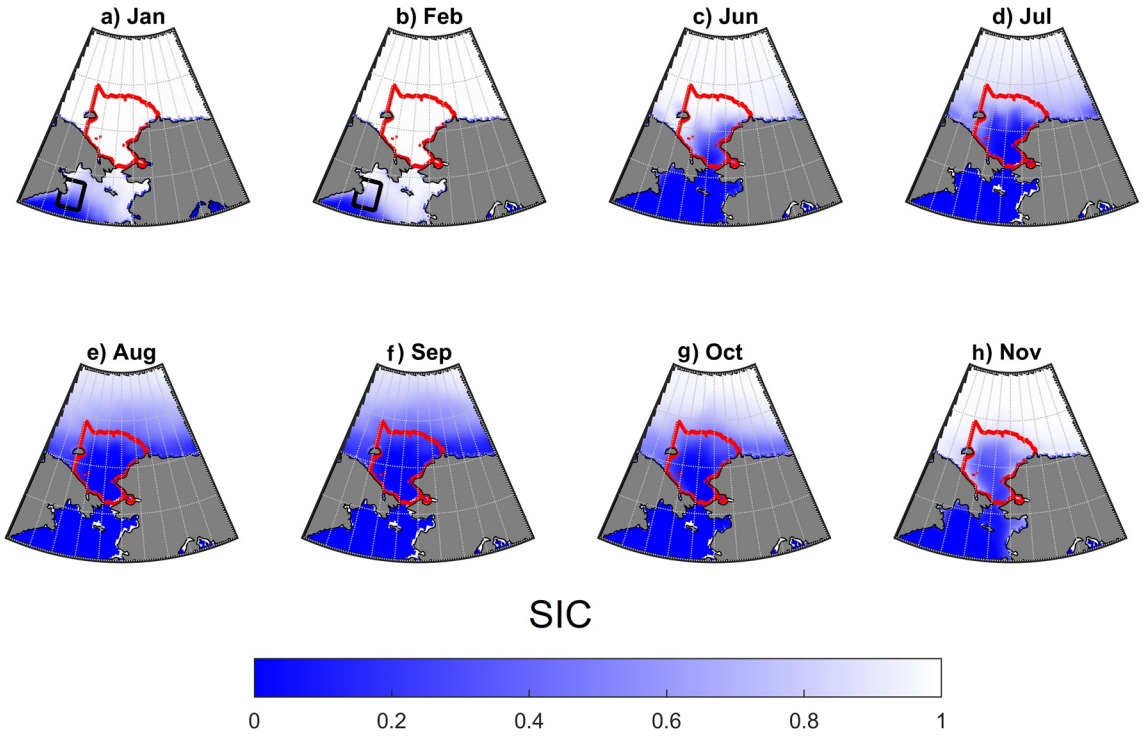

Figure 2. Average sea ice concentrations (SICs) in the Chukchi Sea shelf region (red) over the period 1979–2018. The Cape Navarin (CN) Region (61°N–64°N; 177°W–178°E) is shown in panels (a and b) in black.

derived from OHT variables are, to first order, from the OHT signal itself and not the dynamical influence of Ekman transports on sea ice conditions. To decrease overfitting, additional predictors, e.g., the AO index (National Weather Service, 2020), are only used if they significantly increase model skill as assessed by the adjusted coefficient of determination ($\bar{r}^2$ value). Finally, predictors with standard errors larger than their coefficients are removed. All models meet the following criteria: (1) predictors are linearly independent with variance inflation factors less than 2.5; (2) model residuals are normally distributed; and (3) models are statistically significant at the 95% condifence level ($p < 0.05$). Hereafter, time series modeled using regressions are denoted with a hat (e.g., $\widehat{\mathrm{OHT}}$, $\widehat{\mathrm{T_{vol}}}$, $\widehat{\mathrm{RD}}$, $\widehat{\mathrm{AD}}$) and residuals are calculated as the modeled minus observed value (e.g., $\widehat{\mathrm{OHT}}$ - OHT).

3. Modeling of T_{vol} and OHT

The monthly mean June, July, and September meridional Ekman transport (V_{Ek}) in the ESS is the most important predictor for T_{vol} anomalies of the same months, supporting previous work (Peralta-Ferriz & Woodgate, 2017). For July and September, Bering Sea V_{Ek} and meridional along-strait winds also provide skill, increasing the explained variance of July $\widehat{\mathrm{T_{vol}}}$ from 51% to 63% and September $\widehat{\mathrm{T_{vol}}}$ from 43% to 62%. As noted, the reduced predictive skill of Bering Sea V_{Ek} compared to ESS V_{Ek} is due to a weaker atmospheric forcing in the Bering Sea (Zhang et al., 2020). Weather events introduce noise in all $\widehat{\mathrm{T_{vol}}}$. In the Bering, Chukchi, and ESSs, extratropical cyclones can generate northward or southward continental shelf waves that propagate through the Bering Strait, creating T_{vol} anomalies at synoptic timescales that cannot be captured by monthly Ekman transports or along-strait surface winds (Danielson et al., 2014). In sum, these variables explain 63%, 63% and 62% of June, July, and September T_{vol} variance, respectively (Table 1).

Building $\widehat{\mathrm{OHT}}$ from $\widehat{\mathrm{T_{vol}}}$ necessitates incorporating predictors that capture the temperature of Bering Strait waters. We use the NOAA SST data product averaged over the Bering Sea shelf and the smaller Cape Navarin (CN) region (see Section 2.4; Figures 1 and 2). In the CN region, January 15th through February 15th (JF15) SST anomalies, associated with anomalous local sea ice retreat and increased solar energy uptake, have been linked to the early ice retreat in the Bering Strait via warm water advection along the Anandyr

Table 1
Predictors and Model Coefficients for Final Volume Transport ($\widehat{T_{vol}}$), Ocean Heat Transport ($\widehat{OHT}$), Retreat Date ($\widehat{RD}$), and Advance Date ($\widehat{AD}$) Models

Model	Variables (β)	α	R^2	RMSE	NRMSE
June $\widehat{T_{vol}}$	June ESS V_{Ek} (144.43 ± 25.35 Sv/m/s)	1.32	0.63	0.18 Sv	62%
July $\widehat{T_{vol}}$	July ESS V_{Ek} (150.16 ± 33.84 Sv/m/s)	1.29	0.63	0.18 Sv	66%
	July Bering Sea V_{Ek} (111.64 ± 105.58 Sv/m/s)				
	July V-Bering Strait winds (111.64 ± 59.99 Sv/m/s)				
September $\widehat{T_{vol}}$	Sep ESS V_{Ek} (155.61 ± 49.78 Sv/m/s)	1.03	0.62	0.21 Sv	67%
	Sep Bering Sea V_{Ek} (236.05 ± 174.11 Sv/m/s)				
	Sep V-Bering Strait winds (92.44 ± 41.88 Sv/m/s)				
June $\widehat{OHT}$	June ESS V_{Ek} (1,032.3 ± 733.71 TW/m/s)	15.78	0.47	5.17 TW	77%
	Jan15-Feb15 CN SST (5.30 ± 1.54 TW/°C)				
July $\widehat{OHT}$	July ESS V_{Ek} (3,277.7 ± 1,083.7 TW/m/s)	23.95	0.46	5.92 TW	77%
	Jan15-Feb15 CN SST (5.04 ± 1.76 TW/°C)				
September $\widehat{OHT}$	Sept. ESS V_{Ek} (2,713.6 ± 880.64 TW/m/s)	−4.15	0.79	3.65 TW	49%
	Sept. V-Bering Strait winds (2,067 ± 817.41 TW/m/s)				
	September Bering Sea SST (3.16 ± 0.76 TW/°C)				
$\widehat{RD}$ (June)	June ESS V_{Ek} (−2,078 ± 1,111 Days/m/s)	254.9	0.41	10.2 days	80%
	June Bering Sea SST (−7.06 ± 1.92 Days/°C)				
	Advance date (−0.106 ± 0.064 Days/day)				
$\widehat{RD}$ (JF15)*	Jan15-Feb15 CN SST (−8.31 ± 2.49 Days/°C)	185.4	0.37	8.47 days	82%
$\widehat{AD}$ (September)	Sept. ESS V_{Ek} (6,605.1 ± 1,523.8 Days/m/s)	475.1	0.79	12.8 days	48%
	Sept. Bering Sea SST (6.67 ± 2.18 Days/°C)				
	Retreat date (−1.11 ± 0.19 Days/Day)				
$\widehat{AD}$ (July)	July Bering Sea V_{Ek} (−14677 ± 6,417.3 Days/m/s)	498.5	0.73	14.6 days	54%
	July Bering Sea SST (7.96 ± 2.66 Days/°C)				
	Retreat date (−1.32 ± 0.21 Days/Day)				
	July AO (−8.581 ± 5.25 Days/AO)				

Note: Next to predictor names, coefficients (β) with confidence intervals (±1 standard error) are given. α is the model y-intercept. The model development procedure can be simplified to $V_{Ek} \rightarrow \widehat{T_{vol}} + SST \rightarrow \widehat{OHT} \rightarrow \widehat{RD}$ /$\widehat{AD}$. Predictors with standard errors larger than their coefficients have been removed. * denotes a forecast for years 1998–2018 only. RMSE is the root mean squared error and NRMSE is the RMSE divided by standard deviation of the observed predictant.

current (Luo et al., 2020). Bering Sea SST anomalies are significantly correlated ($p < 0.05$) with both June and September observed near-bottom water temperatures anomalies of the same month (June: $r^2 = 0.29$, September: $r^2 = 0.29$), while July SST anomalies are not significantly correlated with July near-bottom temperature anomalies. In the CN region, JF15 SSTs are significantly correlated with Bering Strait near bottom temperatures in June ($r^2 = 0.44$), July ($r^2 = 0.47$), and September ($r^2 = 0.49$). Thus, CN JF15 SSTs can predict Bering Strait water temperatures at 3.5–7 month lead times.

In June and July, CN JF15 SSTs, along with variables from $\widehat{T_{vol}}$, explains 47% and 46% of June and July OHT variance respectively. September $\widehat{OHT}$ is calculated using Bering Sea SSTs, and along with predictors from $\widehat{T_{vol}}$, explain 79% of OHT variance. Despite the higher correlations in between CN JF15 SSTs and Bering Strait near-bottom water temperatures in September, we utilize September Bering Sea SSTs in the final September $\widehat{OHT}$ to increase explained variance (~4%) and reduce errors (~0.5 TW). While June $\widehat{OHT}$ exhibits a reduced overall fit compared to September $\widehat{OHT}$, both models capture interannual variability described in Woodgate 2018, such as high OHT in 2007 and low OHT in 2012 (see Figure 3).

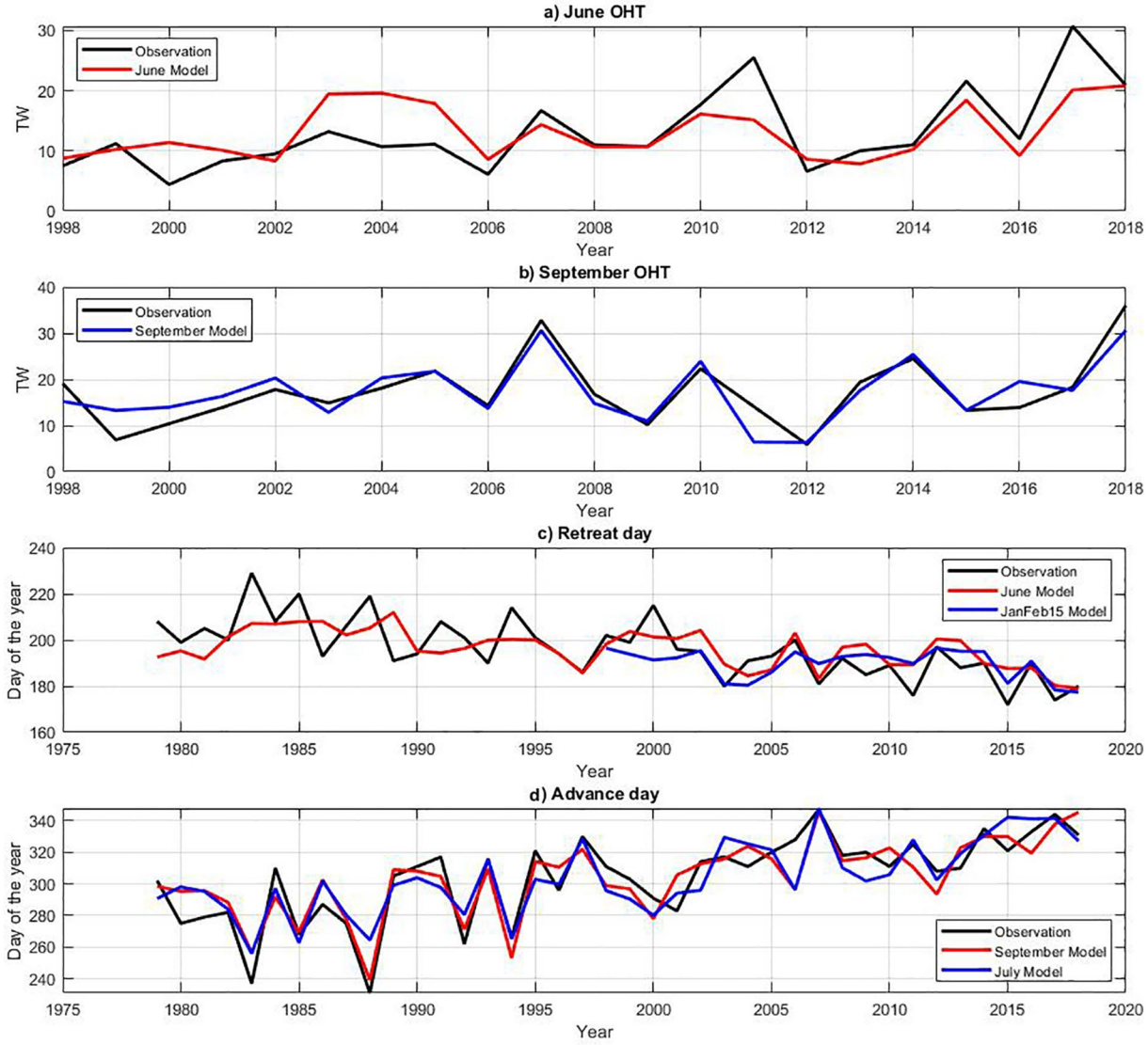

Figure 3. Observed (black) and modeled (a) June ocean heat transports (OHT), (b) September OHT, (c) retreat date (RD), and (d) advance date (AD) from 1979 to 2018. Models with 1-month leads are shown in red and models with 4 month leads are shown in blue. Note the different axes between panels (a, b, c and d). OHT units are terrawatts (TW).

4. Prediction of Retreat and Advance Dates

4.1. Retreat Date Model

JF15 SSTs on their own explain 37% of RD variance with a 4-month lead time, and an root mean squared error (RMSE) of 8.47 days. The downside is that this model is not skillful for the full RD record (1979–2018). In explanation, before the mid-1990s, the CN region was predominantly ice covered between and January 15 and February 15th and SST variability in the region was minimal. In future years, with higher heat content of the Bering Sea limiting sea ice formation (Danielson et al., 2020), SSTs in the CN region may prove to be a consistently skillful predictor.

We thus also present an $\widehat{\mathrm{RD}}$ valid for the entire RD record, using ESS June V_{Ek}, Bering Sea SSTs, and the previous years AD. Predictors from June $\widehat{\mathrm{OHT}}$ (ESS June V_{Ek} and Bering Sea SSTs) explain 37% of RD variability, with the majority of skill coming from Bering Sea SSTs. For $\widehat{\mathrm{RD}}$, the inclusion of Bering Sea SSTs significantly improves model performance beyond the modest relationship between SSTs and Bering Strait water temperatures. This suggests that Bering Sea SSTs impact atmospheric conditions in the Bering and

Chukchi Seas that later influence the RD, despite the limited improvements that SSTs lend to the OHT model. Including the previous year's sea ice advance date further improves $\widehat{RD}$ model skill by 4%. AD anomalies are weakly correlated with RD anomalies of the following year, suggesting that model skill from AD is from information in the positive linear trend of 1.6 days per year, not from increased summer ocean heat uptake (associated with a delayed ice advance) leading to an earlier ice retreat the subsequent spring. The final $\widehat{RD}$ explains 41% of interannual RD variability, with a RMSE of 10.2 days (Table 1, Figure 3). Errors in both $\widehat{RD}$ s are indicative of poor representations of June $\widehat{OHT}$ which are biased against temperature variability relative to T_{vol}, as well as the importance of accurate water temperature information for July sea ice predictions (Lenetsky, et al., 2021).

4.2. Advance Date Model

4.2.1. September Initialization

On their own, variables from September $\widehat{T_{vol}}$ (ESS V_{Ek}, Bering Sea V_{Ek}, V-Bering Strait winds) explain 20% of AD variability. When Bering Sea SSTs are added to variables from September $\widehat{T_{vol}}$ however, $\widehat{AD}$ explains 59% of AD variance. In the final model, we omit Bering Sea V_{Ek} and Sep V-Bering Strait winds because coefficient standard errors are too large (see Section 2.4). Addition of the RD from the previous spring improves the explained variance to 79%, providing information on the linear trend and additional physical processes - an early or late retreat allows for more or less upper ocean heat gain in summer, delaying or speeding autumn ice growth (Serreze et al., 2016). Improved $\widehat{AD}$ explained variance relative to $\widehat{RD}$ corresponds to a more skillful September $\widehat{OHT}$ relative to June $\widehat{OHT}$. Despite the larger explained variance, the best performing $\widehat{AD}$ has larger residuals than $\widehat{RD}$, with an RMSE of 12.8 days. These residuals reflect unpredictable atmospheric processes associated with the ice-albedo feedback not captured by the length of the open water period (Serreze et al., 2016).

4.2.2. July Initialization

To maximize model skill and lead times simultaneously, we also compute $\widehat{AD}$ using variables for July and earlier. Despite the skill of CN SSTs, we use Bering Sea SSTs in this model, as using CN SSTs from February 15 results in reduced skill. Following the same development procedure and variables as before (with ESS V_{Ek} and Sep V-Bering Strait winds removed due to large coefficient errors), we explain 72% of advance date variance with up to a 4-month lead. Including the July AO index to this model then significantly increases explained variance to 73% (see Table 1, Figure 3). Despite not capturing additional physical processes in the volume transport model, the July AO index in $\widehat{AD}$ provides additional information on the atmospheric state which can independently influence the timing of sea ice advance.

With an increase in lead times comes with an increase in error; July $\widehat{AD}$ has a RMSE of 14.6 days. These large residuals reflect anomalous atmospheric events which cannot be captured by OHTs and changes in atmospheric circulations between July and the ice advance, causing the model to misrepresent late summer T_{vol}. Note however, that there is a negative trend in residual size of −0.16 days per year throughout $\widehat{AD}$. This is consistent with the growing importance of the Bering Strait OHT in triggering the ice-albedo feedback (Woodgate et al., 2010).

5. Summary and Conclusion

The lack of real-time observations of Bering Strait waters is an ongoing barrier to forecasting sea ice retreat and advance in the Chukchi Sea. Skillful predictions are possible using physical models initialized with SIC and thickness anomalies (Bushuk et al., 2017; Sigmond et al., 2016), but these forecasts could be significantly improved by inclusion of Bering Strait OHT information (Lenetsky et al., 2021). Our study addresses the data latency problem by developing statistical models that can capture the variability in water volume and OHT through Bering Strait. These models, initialized one month prior to typical retreat and advance, explain 41% and 79% of sea ice retreat and advance date variance with RSMEs of 10.2 and 12.8 days respectively. Forecasts issued at 4-month leads result in only a slight drop in statistical skill, and can respectively capture 37% and 73% of sea ice retreat and advance date variance with RMSEs of 8.5 and 14.6 days. Skillful sea ice

forecasts issued at 4-month lead times will be of advantage to Arctic communities and stakeholders, aiding in operational planning and reducing environmental risks associated with increased marine traffic and resource extraction (Stephenson & Pincus, 2018). As the Arctic Ocean becomes busier in the coming decades, real-time and skillful seasonal sea ice predictions will only continue to grow in importance.

Data Availability Statement

Daily sea ice concentration fields are available at https://nsidc.org/data/NSIDC-0051/versions/1 and ERA5 surface winds are available from https://cds.climate.copernicus.eu/cdsapp#!/dataset/10.24381/cds.f17050d7?tab=overview. Monthly mean ocean heat transport data is available at http://psc.apl.washington.edu/HLD/ and the AO index is available at https://www.cpc.ncep.noaa.gov/products/precip/CWlink/daily_ao_index/ao_index.html. Monthly mean NOAA ERSST and OISST data is from https://psl.noaa.gov/data/gridded/data.noaa.oisst.v2.highres.html and https://psl.noaa.gov/data/gridded/data.noaa.ersst.v5.html.

Acknowledgments
This study was supported by NSF grants PLR 1603914, 1748953 and NASA grant NNX16AJ92G. The authors thank their anonymous reviewers for their constructive feedback.

References

Ahlnas, K., & Garrison, G. (1984). Satellite and oceanographic observations of the warm coastal current in the Chukchi Sea. *Arctic*, *37*(3), 244–254. https://doi.org/10.14430/arctic2197

Banzon, V., Smith, T. M., Chin, T. M., Liu, C., & Hankins, W. (2016). A long-term record of blended satellite and in situ sea-surface temperature for climate monitoring, modeling and environmental studies. *Earth System Science Data*, *8*(1), 165–176. https://doi.org/10.5194/essd-8-165-2016

Birnbaum, G., & Lüpkes, C. (2002). A new parameterization of surface drag in the marginal sea ice zone. *Tellus A: Dynamic Meteorology and Oceanography*, *54*(1), 107–123. https://doi.org/10.3402/tellusa.v54i1.12121

Bushuk, M., Msadek, R., Winton, M., Vecchi, G. A., Gudgel, R., Rosati, A., & Yang, X. (2017). Skillful regional prediction of Arctic sea ice on seasonal timescales. *Geophysical Research Letters*, *44*, 4953–4964. https://doi.org/10.1002/2017GL073155

Cavalieri, D. J., Parkinson, C. L., Gloersen, P., & Zwally, H. J. (1996). *Sea ice concentrations from Nimbus-7 SMMR and DMSP SSM/ISSMIS passive microwave data*. 1978–2007. Boulder, Colorado, USA. National Snow and Ice Data Center. https://doi.org/10.5067/8GQ8LZQVL0VL

Clement, J. L., Maslowski, W., Cooper, L. W., Grebmeier, J. M., & Walczowski, W. (2005). Ocean circulation and exchanges through the northern Bering Sea-1979-2001 model results. *Deep Sea Research Part II: Topical Studies in Oceanography*, *52*(24), 3509–3540. https://doi.org/10.1016/j.dsr2.2005.09.010

Danielson, S. L., Ahkinga, O., Ashjian, C., Basyuk, E., Cooper, L. W., Eisner, L., et al. (2020). Manifestation and consequences of warming and altered heat fluxes over the Bering and Chukchi Sea continental shelves. *Deep Sea Research Part II: Topical Studies in Oceanography*, *177*, 104781. https://doi.org/10.1016/j.dsr2.2020.104781

Danielson, S. L., Weingartner, T. J., Hedstrom, K. S., Aagaard, K., Woodgate, R., Curchitser, E., & Stabeno, P. J. (2014). Coupled wind-forced controls of the Bering-Chukchi shelf circulation and the Bering Strait throughflow: Ekman transport, continental shelf waves, and variations of the Pacific-Arctic sea surface height gradient. *Progress in Oceanography*, *125*, 40–61. https://doi.org/10.1016/j.pocean.2014.04.006

Hersbach, H., Bell, B., Berrisford, P., Hirahara, S., Horányi, A., Muñoz-Sabater, J., et al. (2020). The ERA5 global reanalysis. *Quarterly Journal of the Royal Meteorological Society*, *146*, 1999–2049. https://doi.org/10.1002/qj.3803

Huang, B., Thorne, P. W., Banzon, V. F., Boyer, T., Chepurin, G., Lawrimore, J. H., et al. (2017). *NOAA extended reconstructed sea surface temperature (ERSST), Version 5*. NOAA National Centers for Environmental Information. https://doi.org/10.7289/V5T72FNM

Lenetsky, J. E., Tremblay, B., Brunette, C., & Meneghello, G. (2021). Subseasonal Predictability of Arctic Ocean Sea Ice Conditions: Bering Strait and Ekman-Driven Ocean Heat Transport. *Journal of Climate*, *34*(11), 4449–4462. https://doi.org/10.1175/JCLI-D-20-0544.1

Luo, X., Wang, Y., Lu, Y., Wei, H., Zhao, W., Nie, H., & Hu, X. (2020). A 4-month lead predictor of open-water onset in Bering Strait. *Geophysical Research Letters*, *47*, e2020GL089573. https://doi.org/10.1029/2020GL089573

Lüpkes, C., & Birnbaum, G. (2005). Surface drag in the Arctic marginal sea-ice zone: A comparison of different parameterisation concepts. *Boundary-Layer Meteorology*, *117*(2), 179–211. https://doi.org/10.1007/s10546-005-1445-8

Meneghello, G., Marshall, J., Timmermans, M.-L., & Scott, J. (2018). Observations of seasonal upwelling and downwelling in the Beaufort Sea mediated by sea ice. *Journal of Physical Oceanography*, *48*(4), 795–805. https://doi.org/10.1175/jpo-d-17-0188.1

National Weather Service. (2020). *CPC - monitoring & data: Daily Arctic oscillation index*. https://www.cpc.ncep.noaa.gov/products/precip/CWlink/daily_ao_index/ao_index.html

Paquette, R., & Bourke, R. (1974). Observations on coastal current of Arctic Alaska. *Journal of Marine Research*, *32*(2), 195–207.

Peralta-Ferriz, C., & Woodgate, R. A. (2017). The dominant role of the East Siberian Sea in driving the oceanic flow through the Bering Strait—Conclusions from GRACE ocean mass satellite data and in situ mooring observations between 2002 and 2016. *Geophysical Research Letters*, *44*, 11472–11481. https://doi.org/10.1002/2017GL075179

Pond, S., & Pickard, G. L. (1978). *Introductory dynamic oceanography*. Pergamon Press

Serreze, M. C., Barrett, A. P., Crawford, A. D., & Woodgate, R. A. (2019). Monthly variability in Bering Strait oceanic volume and heat transports, links to atmospheric circulation and ocean temperature, and implications for sea ice conditions. *Journal of Geophysical Research: Oceans*, *124*, 9317–9337. https://doi.org/10.1029/2019JC015422

Serreze, M. C., Crawford, A. D., Stroeve, J. C., Barrett, A. P., & Woodgate, R. A. (2016). Variability, trends, and predictability of seasonal sea ice retreat and advance in the Chukchi Sea. *Journal of Geophysical Research: Oceans*, *121*, 7308–7325. https://doi.org/10.1002/2016JC011977

Serreze, M. C., & Meier, W. N. (2019). The Arctic's sea ice cover: Trends, variability, predictability, and comparisons to the Antarctic. *Annals of the New York Academy of Sciences*, *1436*(1), 36–53. https://doi.org/10.1111/nyas.13856

Sigmond, M., Reader, M. C., Flato, G. M., Merryfield, W. J., & Tivy, A. (2016). Skillful seasonal forecasts of Arctic sea ice retreat and advance dates in a dynamical forecast system. *Geophysical Research Letters*, *43*, 12457–12465. https://doi.org/10.1002/2016GL071396

Smith, T. M., & Reynolds, R. W. (2003). Extended reconstruction of global sea surface temperatures based on COADS Data (1854-1997). *Journal of Climate*, *16*(10), 1495–1510. https://doi.org/10.1175/1520-0442(2003)016<1495:EROGSS>2.0.CO;21

Spall, M. A. (2007). Circulation and water mass transformation in a model of the Chukchi Sea. *Journal of Geophysical Research*, *112*, C05025. https://doi.org/10.1029/2005JC003364

Stephenson, S. R., & Pincus, R. (2018). Challenges of sea-ice prediction for Arctic marine policy and planning. *Journal of Borderlands Studies*, *33*(2), 255–272. https://doi.org/10.1080/08865655.2017.1294494

Timmermans, M. L., Proshutinsky, A., Golubeva, E., Jackson, J. M., Krishfield, R., McCall, M., et al. (2014). Mechanisms of Pacific summer water variability in the Arctic's Central Canada Basin. *Journal of Geophysical Research: Oceans*, *119*, 7523–7548. https://doi.org/10.1002/2014JC010273

United States Navy. (2014). *The United States Navy Artic roadmap for 2014 to 2030* (p. 38). Department of the Navy. https://www.navy.mil/docs/USN_arctic_roadmap.pdf

Woodgate, R. A., Weingartner, T., & Lindsay, R. (2010). The 2007 Bering Strait oceanic heat flux and anomalous Arctic sea-ice retreat. *Geophysical Research Letters*, *37*, L01602. https://doi.org/10.1029/2009GL041621

Woodgate, R. A., Stafford, K. M., & Prahl, F. G. (2015). A synthesis of year-round interdisciplinary mooring measurements in the Bering Strait (1990-2014) and the RUSALCA years (2004-2011). *Oceanography*, *28*(3), 46–67. https://doi.org/10.5670/oceanog.2015.57

Woodgate, R. A. (2018). Increases in the Pacific inflow to the Arctic from 1990 to 2015, and insights into seasonal trends and driving mechanisms from year-round Bering Strait mooring data. *Progress in Oceanography*, *160*, 124–154. https://doi.org/10.1016/j.pocean.2017.12.007

Woodgate, R., & Peralta-Ferriz, C. (2021). Warming and Freshening of the Pacific Inflow to the Arctic From 1990–2019 Implying Dramatic Shoaling in Pacific Winter Water Ventilation of the Arctic Water Column. *Geophysical Research Letters*, *48*(9), https://doi.org/10.1029/2021gl092528

Yang, J. (2006). The seasonal variability of the Arctic Ocean Ekman transport and its role in the mixed layer heat and salt fluxes. *Journal of Climate*, *19*(20), 5366–5387. https://doi.org/10.1175/jcli3892.1

Zhang, K., Wang, T., Xu, M., & Zhang, J. (2019). Influence of wintertime polar vortex variation on the climate over the North Pacific during late winter and spring. *Atmosphere*, *10*(11), 670. https://doi.org/10.3390/atmos10110670

Zhang, W., Wang, Q., Wang, X., & Danilov, S. (2020). Mechanisms driving the interannual variability of the Bering Strait throughflow. *Journal of Geophysical Research: Oceans*, *125*, e2019JC015308. https://doi.org/10.1029/2019JC015308

Erratum

In the originally published version of this article, the unit Days/day was left out of Row 17 of Table 1 and has since been added; in addition, in the first three rows of the table, the expression $\widehat{T_{\mathrm{vol}}}$ has had the hat corrected to match the other instances in the text. The present version may be considered the authoritative version of record.